ACS Catalysis

Research Article

pubs.acs.org/acscatalysis

Enhanced Catalytic Performance of Pt-Free Iron Phthalocyanine by Graphene Support for Efficient Oxygen Reduction Reaction

Yuanyuan Jiang,[†,‡] Yizhong Lu,[§,‡] Xiangyu Lv,*[,†] Dongxue Han,[†] Qixian Zhang,[†] Li Niu,[†] and Wei Chen*[,§]

[†]Engineering Laboratory for Modern Analytical Techniques, [c]/[o] State Key Laboratory of Electroanalytical Chemistry, Changchun Institute of Applied Chemistry, Changchun 130022, Jilin, China

[§]State Key Laboratory of Electroananlytical Chemistry, Changchun Institute of Applied Chemistry, Changchun 130022, Jilin, China

[‡]University of Chinese Academy of Sciences, Beijing, 100039, China

Supporting Information

ABSTRACT: It is commonly accepted that it is almost not possible to realize the large-scale practical application of fuel cells if the expensive noble metal-based electrocatalysts for oxygen reduction reactions (ORR) cannot be replaced by other low-cost, efficient, and stable ones. Herein, our studies demonstrate that iron phthalocyanine (FePc) supported on chemically reduced graphene through $\pi-\pi$ interaction can act as a noble metal-free electrocatalyst with a comparable activity, long-term operation stability, and better tolerance to methanol crossover and CO poisoning compared with commercial Pt/C for ORR in alkaline media. The improved electrochemical activity and stability of FePc by graphene is mainly attributed to the inherent properties of graphene and the π-stacking interaction between FePc and planar aromatic structure of graphene. The as-prepared graphene–iron phthalocyanine (g-FePc) composite exhibits an efficient 4-electron pathway and can be used as a promising Pt-free ORR electrocatalyst.

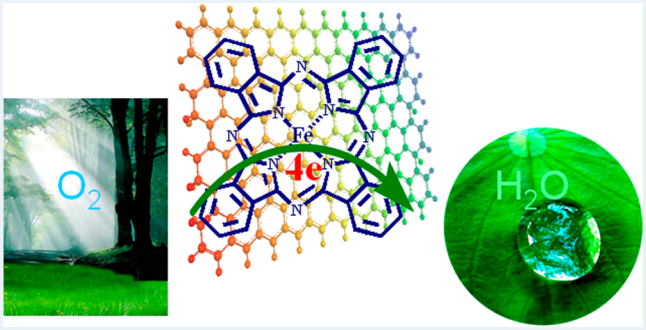

KEYWORDS: *fuel cells, graphene, iron phthalocyanine, noble metal-free electrocatalyst, oxygen reduction reaction*

1. INTRODUCTION

Because of the high power density, high energy-conversion efficiency, and zero or low emission of pollutants, proton exchange membrane fuel cells (PEMFCs) have attracted increasing attention over recent decades; however, the current bottleneck of PEMFCs lies in the sluggish oxygen reduction reaction (ORR) kinetics on the cathode.[1] Although Pt-based electrocatalysts have been traditionally used to catalyze the ORR with a high efficiency, they still suffer from several serious problems, including declining activity, the crossover, and poisoning effects.[2,3] In addition, the high cost of the platinum catalysts, together with its limited reserves in nature, has hindered the large-scale commercialization of PEMFCs.[4] Therefore, various types of nonprecious ORR catalysts have been investigated to replace platinum, including transition metal chalcogenides,[5,6] nitrogen-doped carbon nanotubes or graphene,[7−9] carbon nitride,[10,11] conductive polymer-derived materials,[12,13] and metal-N_4 chelate macrocycles (M-N_4-macrocycles).[14−16] Problems plaguing these catalysts include insufficient activity and low stability.[17] Understanding the nature of ORR catalytic sites on the atomic scale, identifying the causes of instability, and designing catalysts with both optimal activity and durability for ORR are still the big challenges.

Since 1964, when Jasinski first reported that a N_4-chelate complex with a transition metal could be used to electrochemically reduce oxygen,[18] many M-N_4-macrocyclic compounds, such as phthalocyanines and porphyrins, have been widely investigated for ORR,[19−21] among which iron phthalocyanine holds the best performance.[22] In addition, FePc can be synthesized more easily or purchased more cheaply compared with other specially designed metal porphyrins or phthalocyanine. Unfortunately, although much effort has been made for developing FePc as fuel cell catalysts, none of them has reached the level of Pt-based catalysts in terms of catalytic activity and stability.[23]

The poor ORR performance of FePc is mainly attributed to the following aspects: First, FePc molecules are prone to aggregation, which greatly decreases the active sites for ORR. Second, the poor electron conductivity of FePc does not facilitate electron transfer in the ORR process. To solve these problems, their polymeric or heat-treated M-N_4 forms have been fabricated and tested for ORR because this could lead to better chemical and thermal stabilities, higher electronic

Received: March 12, 2013
Revised: April 24, 2013
Published: April 26, 2013

   dx.doi.org/10.1021/cs4001927 | ACS Catal. 2013, 3, 1263−1271

conductivities, and higher O_2 reduction activities; however, such treatments will result in trial and harsh experiments and make it difficult to tailor the structure and the surface properties of the catalysts.[24] In addition, FePc has been studied by supporting on a variety of carbon materials, such as Vulcan XC-72,[25] carbon nanotubes,[26] to improve its catalytic performance. Nevertheless, all of these carbon-supported FePc composites can hardly be dispersed homogeneously in most solvents, and the preparation and purification of carbon nanotubes are really tough process. Moreover, these improvements for the ORR property of FePc are actually limited, so improving the ORR performance of the M-N_4-macrocyclic materials remarkably by a facile and effective way remains to be solved.

This has created the objective for the present work, in which we first synthesized highly stable graphene sheets via mild chemical reduction of exfoliated graphene oxide, then FePc was immobilized onto the graphene sheets through $\pi-\pi$ interaction. The graphene support, to which FePc is homogeneously attached, has improved the dispersibility of indissolvable FePc and acts as supplementary electron-providing sites to prevent issues arising from slow electron transfer. Furthermore, being attached on large planar graphene sheets through forceful $\pi-\pi$ interaction, further aggregation between the FePc molecules is prevented during the storage and the electrochemical tests, maintaining isolation between catalytically active sites. Because of the unique structure and composition, the graphene-iron phthalocyanine (g-FePc) exhibits comparable activity, superior stability, methanol tolerance, and anti-CO poisoning effects compared with a commercial Pt/C catalyst for four-electron ORR in alkaline solution. The desirable performance of the g-FePc composite, together with the low cost and the facile mass-production ability, make the g-FePc a promising cathode candidate for alkaline methanol fuel cell application.

2. EXPERIMENTAL SECTION

2.1. Materials. Iron phthalocyanine (FePc) and 20% E-TEK Pt/C were purchased from Alfa Aesar and used as received. The Vulcan XC-72 carbon support was purchased from Cabot Corporation (Boston, MA, USA). Graphite powder was purchased from Tianjin Guangfu Fine Chemical Research Institute. Unless otherwise stated, other reagents were of analytical grade and used as received. Aqueous solutions were prepared with double-distilled water from a Millipore system (>18 MΩ cm).

2.2. Sample Preparation. Graphene oxide (GO) was synthesized from graphite powder following a modified Hummers' method.[27] Graphene sheets were obtained through the partially reduction of GO by an endogenous reducing agent from a most widely used and cost-effective solvent, without adding any other toxic reducing agent.[28] In a typical experiment, the as-synthesized GO was first dispersed in DMF (0.4 mg/mL) under ultrasonical treatment for 30 min, and then the solution was heated in an oil bath (153 °C) for 45 min. The as-obtained graphene was filtered through a nylon microporous membrane (0.22 μm) and redispersed in DMF with a concentration of 0.4 mg/mL.

To prepare graphene supported FePc, 0.4 mg/mL of the FePc dispersion in DMF was added to the graphene solution of the same concentration drop by drop under stirring. The mixture solution was stirred at room temperature for 6 h and then ultrasonicated for 0.5 h. The obtained g-FePc dispersion was purified by filtration and washing with DMF at least three times and then redispersed in DMF at a concentration of 0.4 mg/mL for further use.

2.3. Characterizations. UV−vis spectroscopic data were collected using a Hitachi U-3900 spectrophotometer, and fluorescence emission spectra were recorded on a Hitachi F-4600 fluorescence spectrophotometer with an excitation wavelength of 490 nm. Transmission electron microscopy (TEM) micrographs were imaged by a JEOL 2000 transmission electron microscopy operating at 100 kV. High-resolution transmission electron microscopy (HRTEM) images were carried out on a JEM-2100 microscopy operated at 200 kV. Energy-dispersive X-ray spectroscopy (EDX) was obtained by a field emission scanning electron microscopy (FE-SEM, XL30ESEM-FEG). XPS measurement was performed on an Thermo ESCALAB 250 spectrometer (Thermo Fishier Scientific, East Grinstead, UK) with Al Kα X-ray radiation as the X-ray source for excitation. Fourier transform infrared spectroscopy (FTIR, Bruker Tensor 27 spectrometer) and Raman spectra (Renishaw Raman system model 1000 spectrometer) with an excitation laser of 514 nm were also used to characterize the samples. Thermogravimetric analyses (TGA) measurements were performed on a Perkin-Elmer TGA-2 thermogravimetric analyzer under nitrogen from room temperature to 900 °C at 10 °C/min.

2.4. Electrochemical Measurements. Cyclic voltammograms (CVs) and amperometric $i-t$ curves were performed with a CHI 660A electrochemical workstation in a conventional 3-electrode system. The working electrode was a 3 mm glassy carbon electrode (GCE) covered with the catalyst samples. A platinum coil and AglAgCl (3 M KCl) electrode were used as the counter electrode and the reference electrode, respectively. All electrode potentials in this work were converted to the reversible hydrogen electrode scale without special description. The CV measurements were conducted in N_2- or O_2-saturated 0.1 M KOH solution at a scan rate of 10 mV/s.

The rotating disk electrode (RDE, d = 5 mm) and rotating ring disk electrode (RRDE) tests were measured on a Princeton Applied Research (PAR) model 636 ring-disk electrode system at a scan rate of 10 mV/s in an O_2-saturated 0.1 M KOH solution. The Pt ring potential was set at 0.5 V (vs AglAgCl) in the RRDE tests. For the RDE and RRDE measurements, 20 μL of the 0.4 mg/mL g--FePc dispersion was pipetted onto the electrode surface, and the electrode was allowed to dry at room temperature. Then 5 μL of 0.5 wt % Nafion was further cast-coated to form a protective layer against catalyst detaching from the electrode surface. In the control experiments, the FePc/C (0.4 mg/mL) was prepared in a way similar to that of the g-FePc, especially that the graphene was substituted by Vulcan XC-72 carbon. A 20 μL portion of the FePc/C ink was drop-coated on the electrodes before the Nafion coating. A 10 μL portion of graphene or FePc solution of the same concentration was coated on the electrode before the Nafion deposition. The Pt/C ink was prepared by mixing 1 mg of commercially available 20% E-TEK Pt/C with 800 μL of water, 190 μL of isopropyl alcohol, and 10 μL of 5 wt % Nafion. A 20 μL portion of the ink was drop-coated on the RDE and RRDE. To remove the capacitive current of the working electrode, the background current was measured by running the above electrodes in N_2-purged KOH electrolyte after the ORR measurements and subtracted from the ORR polarization curve. Therefore, the net faradic current of ORR was obtained for evaluation of the ORR activity.

dx.doi.org/10.1021/cs4001927 | ACS Catal. 2013, 3, 1263−1271

In the CV and $i-t$ measurements, a corresponding amount of catalysts was coated on the GCE (3 mm) with the same catalyst loading per area as that on the RDE.

3. RESULTS AND DISCUSSION

Graphene, a two-dimensional sheet of sp^2 conjugated carbon atoms, has fascinated the scientific community in recent years.[29,30] The combination of a high specific surface area and high electrical conductivity makes graphene sheets highly promising as a supporting platform for electrocatalysts.[31,32] The schematic interaction between graphene and FePc and the ORR process on g-FePc is illustrated in Scheme 1. The

Scheme 1. Schematic Illustration of the Interaction between Graphene and FePc and the ORR Process on g-FePc

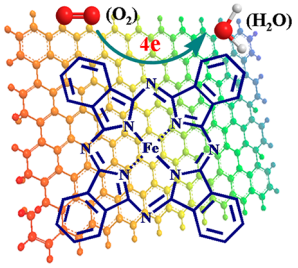

extended, delocalized, and conjugated π-electron system of graphene facilitates interaction with phthalocyanine molecules through the $\pi-\pi$ stacking interaction.[33] Thus, graphene is an ideal selection to support FePc, and the noncovalent binding is an optimal interaction without destroying the intrinsic properties of FePc and graphene. What is more, the presence of graphene can enhance the electrocatalytic response of the FePc centers, which is beneficial for improving the ORR performance of the FePc through a four-electron reaction.

Highly dispersible graphene sheets were obtained by heating the GO solution in DMF. This method has the advantages of low cost because only adopting two easily available materials (GO and DMF), green synthesis without the using of any foreign hazardous reducing agent or stabilizer, and easy preparation make it a suitable method for the large-scale preparation of soluble graphene for practical applications. Figure 1a shows a typical TEM image of a single graphene sheet. It appears transparent and is folded over on one edge with some wrinkles on the sheet. The as-prepared graphene has long-term stability in DMF owing to the residual oxygen-containing groups and the stabilization effect of DMF. After storing for 6 months, the graphene sheets prepared here by the DMF reduction can still maintain homogeneous dispersion, whereas the graphene sheets prepared by the N_2H_4 reduction drastically aggregate (Supporting Information Figure S1a). Free-standing film or graphene paper can be peeled off the filter membrane. This graphene film is bendable and exhibits a shiny metallic luster (Supporting Information Figure S1b). The conductivity of the graphene paper prepared here is tested to be 5800 S/m at room temperature, which is comparable to that of chemically converted graphene paper previously reported.[34] The good dispersibility and high conductivity together with the mass-production property make the as-synthesized graphene sheets terrific supporting material for the FePc. FePc aggregates with a size of 40−50 nm can be uniformly supported on graphene sheets, as can be seen from Figure 1b. The FePc tends to form large aggregates in DMF without the supporting of

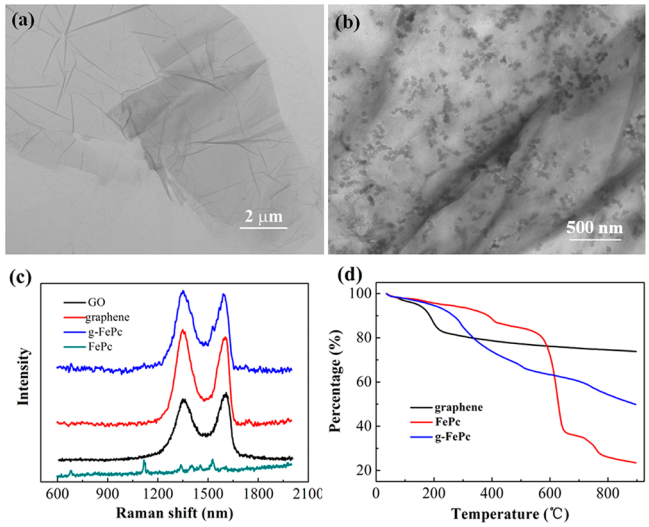

Figure 1. (a) TEM image for the as-synthesized graphene. (b) TEM image of g-FePc composite. (c) Raman spectra of GO, graphene, and g-FePc, and pure FePc. (d) TGA curves of graphene, FePc, and g-FePc with a heating rate of 10 °C/min under nitrogen.

graphene (Supporting Information Figure S1c). From the HRTEM image of g-FePc shown in Supporting Information Figure S1d, it can be seen that the FePc was firmly deposited on the graphene sheets and partly embedded in the sheets. The loading of FePc on graphene prevents the further aggregation of FePc, providing more active sites for the electrocatalysis.

The structural changes that occur during the chemical reduction process from GO to graphene are reflected in their Raman spectra, as seen from Figure 1c. Raman spectroscopy is a sensitive tool to probe the structure of graphene samples.[35,36] The Raman spectrum of GO displays a broad D band peak (the vibrations of carbon atoms with sp^3 electronic configuration of disordered graphene) at ∼1353 cm^{-1} and a G band peak (in-plane vibration of sp^2-bonded carbon atoms) at ∼1604 cm^{-1}. After partial reduction, the two bands become narrower, and the G band shifts to 1601 cm^{-1}. The I_D/I_G ratio of the graphene (1.08) is found to be higher than that of the initial GO (0.90), suggesting a decrease in the average size of the sp^2 domains upon reduction of the exfoliated GO.[37] This may explain why the reduction process can increase the number of small domains of aromaticity responsible for the D peak but not affect their overall size, which is related to the G peak. In addition, compared with graphene, the G band of g-FePc is slightly shifted to 1591 cm^{-1} from 1601 cm^{-1}, This red shift can be ascribed to the extended delocalization of the π electrons, which is a consequence of the $\pi-\pi$ interactions between FePc and graphene.[33,38,39] Moreover, the ratios of the I_D/I_G of graphene (1.08) and g-FePc (1.03) have no apparent difference, which indicates that the interaction between graphene and FePc does not destroy the conjugations of graphene. From the Raman spectra shown in Figure 1c, the Raman intensity of pure FePc is relatively low, and some characteristic peaks are slightly reflected in that of the g-FePc composite. TGA measurements were also carried out to obtain the thermal stability of the partly reduced GO, FePc, and g-FePc. The amount of FePc assembled on graphene has been evaluated by TGA under N_2 atmosphere (Figure 1d). The weight percentage of FePc in g-FePc is calculated to be ∼50% from the mass percentage after 800 °C of the TGA curves.

dx.doi.org/10.1021/cs4001927 | ACS Catal. 2013, 3, 1263−1271

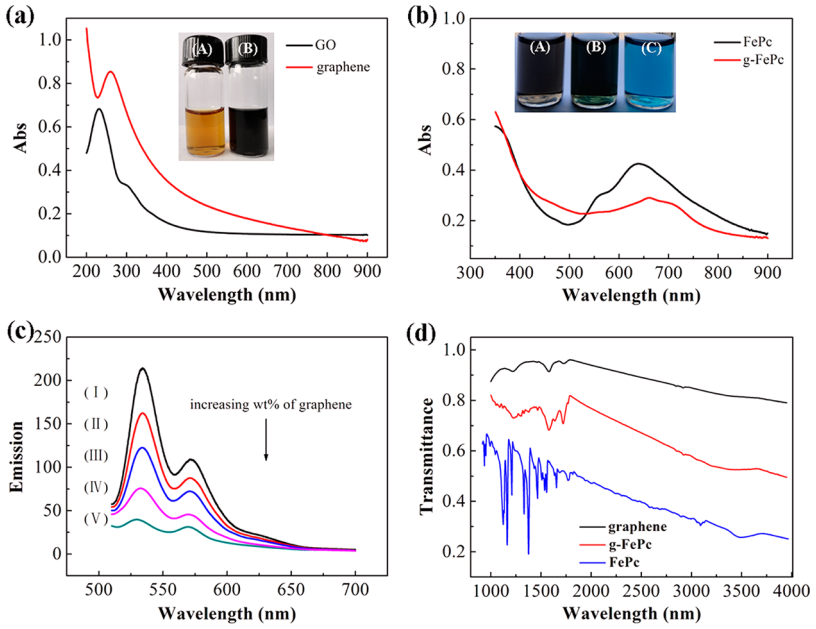

Figure 2. (a) UV−vis absorption spectra of GO and graphene in DMF. Inset: photographs showing the dispersibility of GO and graphene with a concentration of ∼0.8 mg/mL. (b) UV−vis absorption spectra of FePc and g-FePc. The inset contains the images of graphene (A), g-FePc (B) with a concentration of 0.4 mg/mL, and ultrasonic treated FePc (C) in DMF with a concentration of 0.1 mg/mL. (c) Fluorescence spectroscopic changes observed for FePc solution with the increasing wt % of graphene: (I) 0% graphene, (II) 5% graphene, (III) 10% graphene, (IV) 25% graphene, (V) 50% graphene. (d) FTIR spectra of graphene, g-FePc, and FePc.

Figure 2a shows the UV−vis absorption spectra of GO and graphene in DMF solution. The red-shifted $\pi-\pi^*$ absorption band of graphene at 260 nm compared with that of GO at 230 nm is consistent with the partial recovery of the 2D π-conjugated network, showing the reduction of GO occurred as expected.[40] The inset of Figure 2a shows the photographs of GO and the as-prepared graphene dispersion in DMF with a concentration of ∼0.8 mg/mL. Both the GO and graphene can form homogeneous dispersion with the stabilization effect of DMF. The absorption spectra of FePc in DMF before and after the addition of graphene are shown in Figure 2b. The UV−vis spectrum of FePc contains a characteristic Q-band in the near-infrared region centered at 639 nm, a B-band at 329 nm, and a weaker transition at ∼565 nm. The characteristic Q-band is attributed to $\pi-\pi^*$ transition from the highest occupied molecular orbital (HOMO) to the lowest unoccupied molecular orbital (LUMO) of the FePc ring (i.e., from a_{1u} to e_g^* orbitals). The B-band is caused by transitions between a_{2u} and b_{1u} to e_g^* orbitals, and the additional weak vibrational satellite band at ∼565 nm is observed as a result of the inevitable aggregation between the FePc units.[41,42] Regarding the absorption characteristics of FePc, a significant broadening and decrease in intensity dominates the spectrum in the presence of graphene. A closer look reveals that the Q-band shifts from 639 to 659 nm, and a new fingerprint that exhibits a maximum at ∼708 nm appears. The apparent bathochromic shift reflects the strong electronic coupling between the FePc and graphene. It is commonly accepted that the unsubstituted metal phthalocyanine is barely soluble in common solvents. Therefore, much research has focused on synthesizing soluble phthalocyanine by adding hydrophilic functional groups to the molecule; however, the reaction process is really harsh, and the products are usually uncontrollable. In addition, most of the substituted phthalocyanines are not as stable as their unsubstituted counterparts, and their electronic properties are also different from those of the unsubstituted phthalocyanines. The FePc can form dilute solution in DMF after ultrasonication, as shown in the inset of Figure 2b.

After being stored for 1 month, the FePc molecules totally aggregate and sink to the bottom of the bottle, while the graphene sheets and the g-FePc can still maintain a homogeneous dispersion (Supporting Information Figure S2). It has been reported that GO could be used as a functional dispersing agent for graphite powders and carbon nanotubes, which are known to be difficult to process in water through $\pi-\pi$ interaction.[43,44] Inspired by the surfactant behaviors of GO for the dispersion of graphite and carbon nanotubes, we conclude that the partially reduced graphene sheets (seen from the FTIR in Figure 2d and XPS results in Supporting Information Figure S3) here could also act as a dispersing agent and improve the dispersion of the π-conjugated FePc molecules. The loading of FePc on graphene enlarges the distance between the graphene sheets and, in return, stabilizes the dispersion of graphene.

Fluorescence spectra of the FePc solution in DMF with the gradual addition of graphene were recorded to examine the electronic interactions between graphene and FePc (Figure 2c). The observed luminescence quenching of the FePc by the gradual addition of graphene reveals that there is a strong interaction between the excited state of FePc and the graphene in the composite. The fluorescence quenching of the excited FePc by graphene is probably associated with photoinduced electron transfer.[45]

The functional groups present in the starting materials and the hybrid were characterized by FTIR. As shown in Figure 2d, after reduction of GO in DMF, the adsorption bands of C−OH (deformation of hydroxyl) at 1352 cm^{-1}, C−O (epoxy or alkoxy) at 1050 cm^{-1}, and C−OH (vibration of hydroxyl) around 3380 cm^{-1} disappear. The intensities of absorption bands of C═O (in carboxylic species) at 1720 cm^{-1}, and C−

dx.doi.org/10.1021/cs4001927 | ACS Catal. 2013, 3, 1263−1271

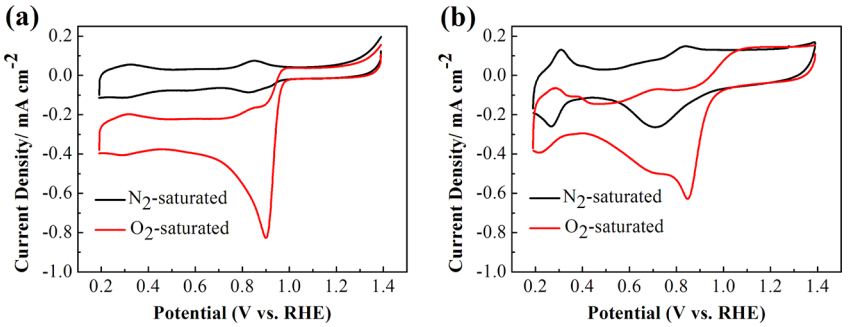

Figure 3. Cyclic voltammetry curves of ORR on the g-FePc (a) and Pt/C (b) electrodes in N_2- and O_2-saturated 0.1 M KOH at a scan rate of 10 mV/s.

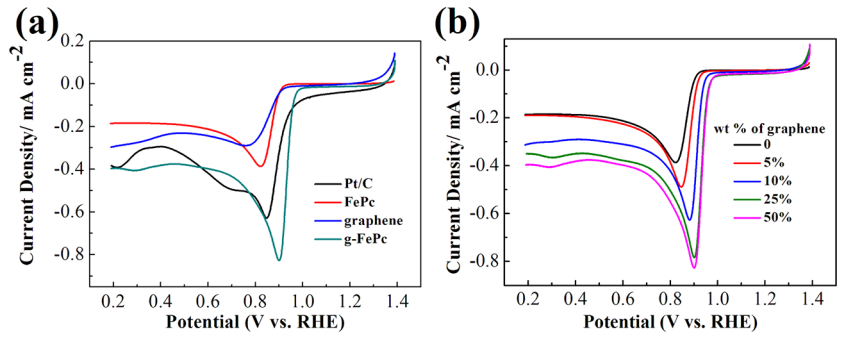

Figure 4. (a) Reduction of oxygen on Pt/C, FePc, graphene, and g-FePc electrodes in O_2-saturated 0.1 M KOH. Scan rate: 10 mV/s. (b) Linear sweep voltammogram of g-FePc with different mass ratios of graphene in O_2-saturated 0.1 M KOH with a scan rate of 10 mV/s.

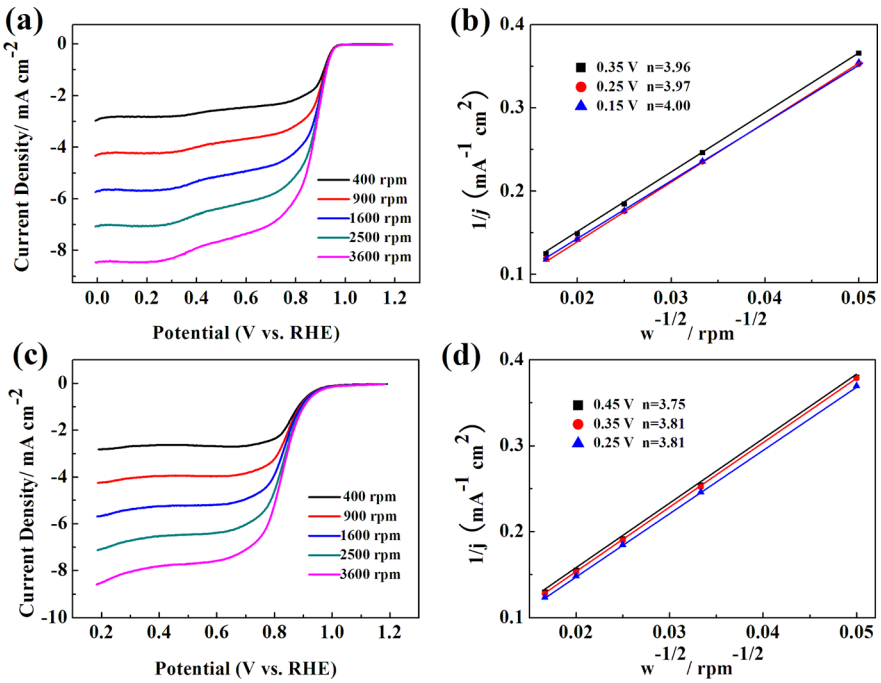

Figure 5. Rotating disk electrode linear sweep voltammograms tests obtained for g-FePc (a) and Pt/C (c) at various speeds. Koutecky–Levich plots for g-FePc (b) and Pt/C (d) obtained from RDE measurements in parts a and c, respectively. The transferred electron number per oxygen molecule in the ORR is calculated and listed after each potential.

O–C (epoxy species) at 1225 cm^{-1} greatly decrease but still remain.[46] The C 1s XPS spectra of GO and graphene confirm the residual of some oxygen-containing species (Supporting Information Figure S3a, b). These results prove that GO was partially reduced to graphene. The FTIR spectrum of the purified g-FePc (by repeatedly washing with DMF to eliminate the possible existence of mixture) resembles that of graphene, with the presence of most of the fingerprints of FePc, suggesting the formation of a graphene and FePc composite. The N 1s XPS spectra of purified g-FePc also present the peak information of both graphene and FePc (Supporting

dx.doi.org/10.1021/cs4001927 | ACS Catal. 2013, 3, 1263–1271

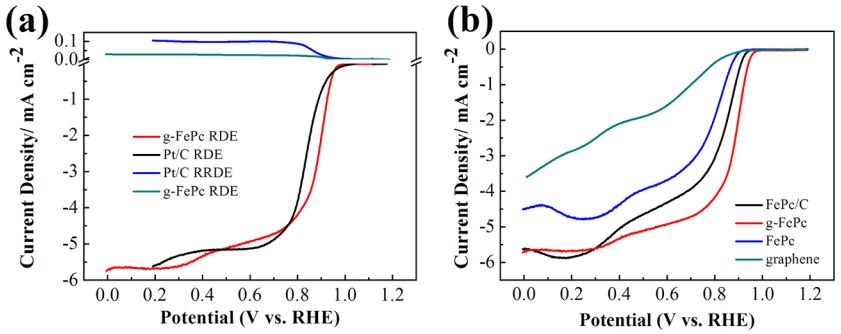

Figure 6. (a) RDE measurements of oxygen reduction (negative current) and RRDE measurements of hydrogen peroxide oxidation (positive current) on g-FePc and Pt/C electrodes in O_2-saturated 0.1 M KOH. The ring electrode is polarized at 0.5 V (vs Ag|AgCl). Rotation rate: 1600 rpm. Scan rate: 10 mV/s. (b) Comparison of the RDE polarization curves of FePc/C, g-FePc, FePc, and graphene in O_2-saturated 0.1 M KOH at 1600 rpm.

Information Figure S3d–f), which also indicates the formation of the g-FePc composite.

Supporting Information Figure S4a shows the survey XPS data of the g-FePc. The peaks of C, N, O, Fe can be obviously found, revealing that the FePc molecules have been successfully anchored on the graphene surface. The EDX spectrum of g-FePc also suggests the presence of C, N, O, and Fe elements with the peak of Si from the silicon wafer. The oxygen peak is from the partially reduced graphene oxide. The element analysis by EDX (mean value of five measurements) in the inset of Supporting Information Figure S4b shows that the mass percentage of Fe in the composite is ~5.5%, from which the FePc mass percentage in the composite can been figured out, and the result is in accordance with the TGA tests, suggesting that most of the used FePc have been successfully loaded on the graphene sheets. The Fe $2p_{3/2}$ peak is centered at 709.4 eV, and the Fe $2p_{1/2}$ peak is located at 722.8 eV in FePc (Supporting Information Figure S4c), which is in agreement with the previously reported values.[42,47] Compared with the FePc molecule, the Fe $2p_{3/2}$ and Fe $2p_{1/2}$ values of the g-FePc shifted to 711.5 and 725 eV, respectively (Supporting Information Figure S4d), suggesting the interaction between graphene and FePc leads to a decrease in the electron density on the Fe atom. The XPS results agree well with the Raman measurements.

To gain insight into the ORR activity of the g-FePc, the cyclic voltammogram (CV) measurements of the g-FePc modified electrode were measured in 0.1 M KOH solution (Figure 3). Commercial 20 wt % platinum on Vulcan carbon black (Pt/C from E-TEK) was also studied as a control experiment. In Figure 3a, the g-FePc exhibits a pronounced cathodic ORR peak at 0.90 V in O_2-saturated KOH, which is even more positive than that of commercial Pt/C (0.85 V in Figure 3b), and the current density is also larger than that obtained from the Pt/C electrode with the same catalyst loading (the same mass amount of FePc and Pt). The ORR peak potential of g-FePc is 80 and 140 mV more positive than those of FePc and graphene, respectively, and the current density for g-FePc is more than twice as large as those of the FePc and graphene catalysts (Figure 4a). The markedly improved ORR activity of g-FePc composite compared with the single component might be attributed to the synergistic effect (strong interaction) between FePc and graphene. We also find that with the loading percentage of FePc in the composite increasing, the ORR activity of the g-FePc elevates. When the mass ratio of FePc reaches 50%, the improvement of the ORR activity becomes inconspicuous (Figure 4b), so 50 wt % FePc loading is chosen for the following experiments.

To further investigate the reaction kinetics of the catalysts during ORR, linear sweep voltammetry measurements on a rotating disk electrode were carried out for each of the electrode materials in O_2-saturated 0.1 M KOH. A set of polarization curves for the ORR on g-FePc recorded from 400 to 3600 rpm are displayed in Figure 5a. These polarization curves show typical increasing current with higher rotation speeds, which can be explained by shortened diffusion distance at high speeds. The Koutecky–Levich plots (j^{-1} vs $\omega^{-1/2}$; see below) can be obtained from the polarization curve at different potentials (Figure 5b). The linearity of the Koutecky–Levich plots and near parallelism of the fitting lines suggest first-order reaction kinetics toward the concentration of dissolved oxygen and a similar electron transfer number for ORR at different potentials.

The transferred electron number per oxygen molecule involved in the oxygen reduction at each of the electrodes is determined by the Koutecky–Levich equation given below:[48]

$$\frac{1}{j} = \frac{1}{j_k} + \frac{1}{B\omega^{0.5}} \quad (1)$$

$$B = 0.2nF(D_0)^{2/3}\nu^{-1/6}C_0 \quad (2)$$

where j is the measured current density, j_k is the kinetic current density, ω is the electrode rotating rate, n represents the number of electrons transferred per oxygen molecule, F is the Faraday constant (F = 96 485 C mol^{-1}), D_0 is the diffusion coefficient of O_2 in 0.1 M KOH (1.9×10^{-5} cm^2/s), ν is the kinetic viscosity (0.01 cm^2/s), and C_0 is the bulk concentration of O_2 (1.2×10^{-6} mol/cm^3).[49] The constant 0.2 is used when the rotation speed is expressed in rpm. According to eqs 1 and 2, the number of transferred electrons can be obtained from the slope of the Koutecky–Levich plots. The electron transfer numbers from the slopes of Koutecky–Levich plots are calculated to be 3.96, 3.97, and 4.00 at 0.35, 0.25, and 0.15 V, respectively, suggesting that the g-FePc catalyst exhibits a dominant four-electron oxygen reduction process, similar to ORR catalyzed by a commercial Pt/C catalyst (Figure 5d).

An additional method to estimate n and to further verify the ORR pathways is the RRDE technique, in which H_2O_2 produced at the disk electrode can be detected by the ring electrode. Figure 6a shows the disk and ring current for the g-FePc hybrid catalysts, and the results from Pt/C catalyst are also given for comparison. In the RDE measurements, the onset

dx.doi.org/10.1021/cs4001927 | ACS Catal. 2013, 3, 1263–1271

potential of ORR on g-FePc is comparable to that on Pt/C. Meanwhile, the half-wave potential ($E_{1/2}$) on g-FePc is more positive than that from the commercial Pt/C catalyst (~50 mV positive shift compared with the Pt/C catalyst). In addition, the diffusion-limiting current of g-FePc hybrids is almost comparable to that of Pt/C catalyst with the same catalyst loading (the same mass amount of Pt and FePc). To verify the ORR catalytic pathways of these catalysts, RRDE measurements were carried out to monitor the formation of peroxide species (HO_2^-) during the ORR process. The percentage of HO_2^- and the electron transfer number are determined by the following equations:[50]

$$HO_2^-\% = 200 \times \frac{i_R/N}{i_D + i_R/N} \quad (3)$$

$$n = 4 \times \frac{i_D}{i_D + i_R/N} \quad (4)$$

where i_D is the disk current, i_R is the ring current, and N is the current collection efficiency of the Pt ring. N was determined to be 0.36 from the reduction of $K_3Fe[CN]_6$, which is consistent with the manufacturer's value (0.37). As is calculated from Figure 6a, the HO_2^- percentage produced by the g-FePc is below 3% (obtained from eq 3), even lower than that of the Pt/C. The RRDE tests agree well with our results calculated from the Koutecky–Levich equation that the ORR electron transfer number for g-FePc is close to 4 (based on eq 4).

The RDE measurements for the FePc and graphene electrocatalyst were also carried out in our experiments. As seen from Supporting Information Figure S5, FePc itself has good ORR activity with the electron transfer number of ~3.7. Graphene also has an ORR response, but its activity is less than desirable. The numbers of electrons transferred per O_2 molecule for graphene is calculated to be 2.56, 2.99, and 3.21 at 0.35, 0.25, and 0.15 V, respectively (Supporting Information Figure S6). This suggests that the oxygen reduction on graphene electrocatalyst may proceed by a coexisting pathway involving both the two-electron and four-electron transfers. We have also compared the ORR performance of the g-FePc with the conventional carbon-supported FePc electrocatalyst with the same catalyst loading. Although the FePc/C has better ORR activity than FePc, they are still not as good as the g-FePc (Figure 6b and Supporting Information Figure S7). Moreover, the FePc/C is hardly dispersible in most solvents, which limits its practical application, and the current density loss on the FePc/C catalyst was more than 50% after a chronoamperometric test for 10000 s (Supporting Information Figure S8). These control experiments demonstrate that the graphene support can markedly improve the ORR performance of the FePc catalyst. Although previous reports of the carbon nanotube-supported FePc also exhibited some interesting performance, the stability of these composites was still not clear.[22,26] In addition, our graphene support outperforms the carbon nanotube support in the aspect of facile and low-cost production in a large scale. FePc supported on N-doped graphene has also been recently reported as a catalyst;[51] however, the more complicated preparation processes in this report render it unsuitable for large-scale preparation, and the interaction between graphene and FePc was not investigated systematically in the study. We also compare our catalyst with some recently reported non-noble metal catalysts that have admirable performance for the cathodic ORR (seen in Supporting Information Table S1). In general, the performance of our g-FePc catalyst is comparable to, or even better than, those of the top reports in the aspect of onset potential and half-wave potential.

In addition to catalyst activity, stability and tolerance to crossover and poison effects are also critical issues in fuel cell applications. To investigate the stability of the g-FePc for ORR, we held the electrodes at 0.85 V for 10000 s in a 0.1 M KOH solution saturated with oxygen under stirring. The corresponding chronoamperometric response of g-FePc and Pt/C are shown in Figure 7a. As can be seen, a high relative current of

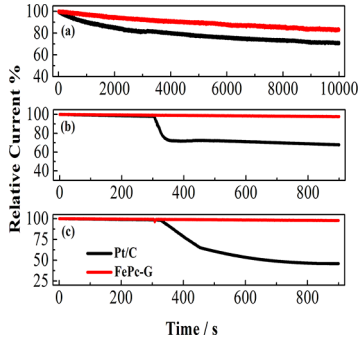

Figure 7. (a) Current–time chronoamperometric response of g-FePc and Pt/C in O_2-saturated 0.1 M KOH under stirring. Current–time chronoamperometric response of g-FePc and Pt/C in O_2-saturated 0.1 M KOH with a rapid addition of 3 M methanol (b), and gradual introduction of CO (c) at around 300 s with a rotation rate of 1600 rpm.

84.0% for g-FePc is preserved after the operation, whereas the relative current of Pt/C catalyst decreases to 71.6%. This indicates that the stability of g-FePc is better than that of the commercial Pt/C electrode. The stability tests based on the potential cycling were also conducted. As seen in Supporting Information Figure S9a, after 500 potential cycles of g-FePc in 0.1 M O_2-saturated KOH, the obtained ORR polarization curve displayed only a 3.87% decrease in the current density at 0.2 V, and the half-wave potential ($E_{1/2}$) exhibited a negative shift of ~25 mV. In contrast, the carbon-supported FePc (FePc/C) exhibited an ~50% loss of the initial current density after only 100 potential cycles (Supporting Information Figure S9b). The results strongly indicate that the stability of FePc has been greatly improved by using graphene sheets as supports; however, despite the elevated stability of g-FePc, there is still a long way to go to further improve its stability for practical applications in fuel cells.

The g-FePc catalyst was further subjected to testing the possible methanol crossover and carbon monoxide (CO) poison effects. A sharp decrease in current upon the addition of 3 M methanol was observed for the Pt/C electrode (Figure 7b). In contrast, the amperometric response from the g-FePc electrode remained almost unchanged after the addition of methanol, indicating a better methanol tolerance than the commercial Pt/C electrocatalyst. As for the CO poison effect shown in Figure 7c, the g-FePc electrode is insensitive to CO, whereas the Pt/C electrode is gradually poisoned with the gradual addition of CO to the O_2-saturated KOH. These results indicate that the g-FePc catalyst has terrific selectivity for ORR and high CO tolerance.

In general, several combined features of graphene support may contribute to the ORR performance enhancement. First,

dx.doi.org/10.1021/cs4001927 | ACS Catal. 2013, 3, 1263–1271

compared with other supports, graphene sheets provide a unique 2D support with a large open and accessible surface area; therefore, the diffusion of the reactant and product away from the catalytic centers is much easier, as found in a similar composite structure of graphene-supported hemin.[52] Second, the excellent electron transfer ability of graphene is favorable for charge transfer during the ORR. Moreover, partially reduced graphene sheets have stabilization and solubilization effects on FePc through strong $\pi-\pi$ interaction, which provides more active sites and improves the stability of the FePc.

4. CONCLUSIONS

In summary, highly soluble graphene was synthesized in large scale by a facile and cost-effective method, and a graphene-FePc composite was then further constructed through forceful $\pi-\pi$ interaction. The as-prepared g-FePc catalyst possesses prominent ORR catalytic activity, which is comparable with commercial Pt/C in both onset potential and current density toward ORR. Furthermore, its half-wave potential in the RDE measurements is ~50 mV more positive than that of the commercial Pt/C catalyst. As a noble metal-free electrocatalyst, the g-FePc shows significantly reduced methanol crossover effects, an anti-CO poisoning effect, and better stability than the commercial Pt/C in alkaline medium. The inherent low stability of the commonly investigated FePc supported by carbon is improved by the graphene support without using the traditional pyrolization method. The improved ORR performance of FePc by graphene could be attributed to the increased dispersibility of FePc on graphene sheets with more active sites exposed and the facilitated electron transfer in the ORR by the graphene support.

■ ASSOCIATED CONTENT

Supporting Information

Additional structural characterizations and electrochemical measurements are shown in Figures S1–S9. This material is available free of charge via the Internet at http://pubs.acs.org.

■ AUTHOR INFORMATION

Corresponding Author

*E-mails: (W.C.) weichen@ciac.jl.cn, (X.L.) lvxiangyu@ciac.jl.cn.

Notes

The authors declare no competing financial interest.

■ ACKNOWLEDGMENTS

The authors are most grateful to the NSFC, China (Nos. 21175130, 21105096, 21205112, and 21275136) and the Department of Science and Techniques of Jilin Province (Nos. 20120308, 201215090, and 201215091) for their financial support.

■ REFERENCES

(1) Steele, B. C. H.; Heinzel, A. *Nature* **2001**, *414*, 345–352.
(2) Winter, M.; Brodd, R. J. *Chem. Rev.* **2004**, *104*, 4245–4270.
(3) Rabis, A.; Rodriguez, P.; Schmidt, T. J. *ACS Catal.* **2012**, *2*, 864–890.
(4) Su, D. S.; Sun, G. *Angew. Chem., Int. Ed.* **2011**, *50*, 11570–11572.
(5) Gong, K.; Yu, P.; Su, L.; Xiong, S.; Mao, L. *J. Phys. Chem. C.* **2007**, *111*, 1882–1887.
(6) Feng, Y.; He, T.; Alonso-Vante, N. *Chem. Mater.* **2007**, *20*, 26–28.
(7) Gong, K.; Du, F.; Xia, Z.; Durstock, M.; Dai, L. *Science* **2009**, *323*, 760–764.
(8) Geng, D.; Chen, Y.; Chen, Y.; Li, Y.; Li, R.; Sun, X.; Ye, S.; Knights, S. *Energy Environ. Sci.* **2011**, *4*, 760–764.
(9) Wang, H.; Maiyalagan, T.; Wang, X. *ACS Catal.* **2012**, *2*, 781–794.
(10) Liang, J.; Zheng, Y.; Chen, J.; Liu, J.; Hulicova-Jurcakova, D.; Jaroniec, M.; Qiao, S. Z. *Angew. Chem., Int. Ed.* **2012**, *51*, 3892–3896.
(11) Zheng, Y.; Jiao, Y.; Chen, J.; Liu, J.; Liang, J.; Du, A.; Zhang, W.; Zhu, Z.; Smith, S. C.; Jaroniec, M.; Lu, G. Q.; Qiao, S. Z. *J. Am. Chem. Soc.* **2011**, *133*, 20116–20119.
(12) Yuan, X.; Zeng, X.; Zhang, H.-J.; Ma, Z.-F.; Wang, C.-Y. *J. Am. Chem. Soc.* **2010**, *132*, 1754–1755.
(13) Olson, T. S.; Pylypenko, S.; Atanassov, P.; Asazawa, K.; Yamada, K.; Tanaka, H. *J. Phys. Chem. C.* **2010**, *114*, 5049–5059.
(14) Gojkovic, S. L.; Gupta, S.; Savinell, R. F. *J. Electroanal. Chem.* **1999**, *462*, 63–72.
(15) Harnisch, F.; Wirth, S.; Schroeder, U. *Electrochem. Commun.* **2009**, *11*, 2253–2256.
(16) Chen, R.; Li, H.; Chu, D.; Wang, G. *J. Phys. Chem. C.* **2009**, *113*, 20689–20697.
(17) Jaouen, F.; Proietti, E.; Lefevre, M.; Chenitz, R.; Dodelet, J.-P.; Wu, G.; Chung, H. T.; Johnston, C. M; Zelenay, P. *Energy Environ. Sci.* **2011**, *4*, 114–130.
(18) Jasinski, R. *Nature* **1964**, *201*, 1212–1213.
(19) Zhang, L.; Zhang, J. J.; Wilkinson, D. P.; Wang, H. J. *J. Power Sources* **2006**, *156*, 171–182.
(20) Samanta, S.; Sengupta, K.; Mittra, K.; Bandyopadhyay, S.; Dey, A. *Chem. Commun.* **2012**, *48*, 7631–7633.
(21) Li, W.; Yu, A.; Higgins, D. C.; Llanos, B. G.; Chen, Z. *J. Am. Chem. Soc.* **2010**, *132*, 17056–17058.
(22) Morozan, A.; Campidelli, S.; Filoramo, A.; Jousselme, B.; Palacin, S. *Carbon.* **2011**, *49*, 4839–4847.
(23) Morozan, A.; Jousselme, B.; Palacin, S. *Energy Environ. Sci.* **2011**, *4*, 1238–1254.
(24) Bezerra, C. W. B.; Zhang, L.; Liu, H.; Lee, K.; Marques, A. L. B.; Marques, E. P.; Wang, H.; Zhang, J. *J. Power Sources* **2007**, *173*, 891–908.
(25) Baranton, S.; Coutanceau, C.; Roux, C.; Hahn, F.; Leger, J. M. *J. Electroanal. Chem.* **2005**, *577*, 223–234.
(26) Dong, G.; Huang, M.; Guan, L. *Phys. Chem. Chem. Phys.* **2012**, *14*, 2557–2559.
(27) Hummers, W. S.; Offeman, R. E. *J. Am. Chem. Soc.* **1958**, *80*, 1339–1339.
(28) Ai, K.; Liu, Y.; Lu, L.; Cheng, X.; Huo, L. *J. Mater. Chem.* **2011**, *21*, 3365–3370.
(29) Guo, S.; Dong, S. *Chem. Soc. Rev.* **2011**, *40*, 2644–2672.
(30) Huang, X.; Qi, X.; Boey, F.; Zhang, H. *Chem. Soc. Rev.* **2012**, 41.
(31) Jiang, Y.; Zhang, X.; Shan, C.; Hua, S.; Zhang, Q.; Bai, X.; Dan, L.; Niu, L. *Talanta* **2011**, *85*, 76–81.
(32) Jiang, Y.; Lu, Y.; Li, F.; Wu, T.; Niu, L.; Chen, W. *Electrochem. Commun.* **2012**, *19*, 21–24.
(33) Geng, J.; Jung, H.-T. *J. Phys. Chem. C.* **2010**, *114*, 8227–8234.
(34) Li, D.; Muller, M. B.; Gilje, S.; Kaner, R. B.; Wallace, G. G. *Nat. Nanotechnol.* **2008**, *3*, 101–105.
(35) Rao, C. N. R.; Sood, A. K.; Subrahmanyam, K. S.; Govindaraj, A. *Angew. Chem., Int. Ed.* **2009**, *48*, 7752–7777.
(36) Allen, M. J.; Tung, V. C.; Kaner, R. B. *Chem. Rev.* **2009**, *110*, 132–145.
(37) Stankovich, S.; Dikin, D. A.; Piner, R. D.; Kohlhaas, K. A.; Kleinhammes, A.; Jia, Y.; Wu, Y.; Nguyen, S. T.; Ruoff, R. S. *Carbon.* **2007**, *45*, 1558–1565.
(38) Das, B.; Voggu, R.; Rout, C. S.; Rao, C. N. R. *Chem. Commun.* **2008**, 5155–5157.
(39) Voggu, R.; Rout, C. S.; Franklin, A. D.; Fisher, T. S.; Rao, C. N. R. *J. Phys. Chem. C* **2008**, *112*, 13053–13056.
(40) Zhang, X.-F.; Xi, Q. *Carbon.* **2011**, *49*, 3842–3850.
(41) Ghani, F.; Kristen, J.; Riegler, H. *J. Chem. Eng. Data* **2012**, *57*, 439–449.

(42) Chamlek, O.; Pratontep, S.; Kerdcharoen, T.; Osotchan, T. *Smart Mater.* **2008**, *55*−*57*, 301−304.
(43) Kim, J.; Cote, L. J.; Kim, F.; Yuan, W.; Shull, K. R.; Huang, J. *J. Am. Chem. Soc.* **2010**, *132*, 8180−8186.
(44) Kim, J.; Cote, L. J.; Huang, J. *Acc. Chem. Res.* **2012**, *45*, 1356−1364.
(45) Matte, H. S. S. R.; Subrahmanyam, K. S.; Rao, K. V.; George, S. J.; Rao, C. N. R. *Chem. Phys. Lett.* **2011**, *506*, 260−264.
(46) Gao, H.; Xiao, F.; Ching, C. B.; Duan, H. *ACS Appl. Mater. Interfaces* **2011**, *3*, 3049−3057.
(47) Uchida, K.; Soma, M.; Onishi, T.; Tamaru, K. *Inorg. Chim. Acta* **1978**, *26*, L3−L4.
(48) Bard, A. J.; Faulkner, L. R. *Electrochemical Methods: Fundamentals and Applications*, 2nd ed.; Wiley: New York, 2001, pp 235−237.
(49) Chen, W.; Chen, S. *Angew. Chem., Int. Ed.* **2009**, *48*, 4386−4389.
(50) Ma, G.; Jia, R.; Zhao, J.; Wang, Z.; Song, C.; Jia, S.; Zhu, Z. *J. Phys. Chem. C.* **2011**, *115*, 25148−25154.
(51) Zhang, C.; Hao, R.; Yin, H.; Liu, F.; Hou, Y. *Nanoscale* **2012**, *4*, 7326−7329.
(52) Xue, T.; Jiang, S.; Qu, Y.; Su, Q.; Cheng, R.; Dubin, S.; Chiu, C.-Y.; Kaner, R.; Huang, Y.; Duan, X. *Angew. Chem. Int. Ed.* **2012**, *51*, 3822−3825.